J Nanopart Res (2016)18:71
DOI 10.1007/s11051-016-3383-4

RESEARCH PAPER

The surface interactions of a near-neutral carbon nanoparticle tracer with calcite

Yan Vivian Li · Lawrence M. Cathles

Received: 26 October 2015 / Accepted: 24 February 2016

Abstract A new class of nearly charge-neutral carbon-cored nanoparticle tracers are remarkably non-interactive with solid surfaces and could provide a valuable baseline for diverse hydrological and environmental studies of subsurface flow and particle transport. We investigate the causes of inertness by studying the interactions with calcite of a nanoparticle of this class synthesized from malic acid and ethanolamine (M-dots) dispersed in brine (NaCl, $CaCl_2$, and $MgCl_2$) solutions. None of the M-dots are retained in calcite sand-packed columns when dispersed in DI water. Dispersed in the NaCl and mixed brine solutions, 5.6 % of and 7.3 % of the M-dots are initially retained, but 65 and 13 % of these retained particles are subsequently released when the column is flushed with DI water. When dispersed in the $CaCl_2$ and $MgCl_2$ solutions, 65 and 54 % of the M-dots are initially retained, and 28 and 26 % subsequently released in the DI water flush. The M-dots have a small negative zeta potential in all solutions, but the calcite zeta potential changes from strongly negative to strongly positive across the solution series, and the particle retention tracks this change. Derjaguin–Landau–Verwey–Overbeek (DLVO) modeling of the force between a calcite probe and an M-dot coated surface shows that hydration forces repel the particles in the DI water, NaCl, and mixed solutions, but not in the $CaCl_2$ and $MgCl_2$ solutions. These results show that near-zero charge and strongly hydrophilic decoration are the causes of the remarkable inertness of carbon-cored nanoparticles, and also suggest that nanoparticles could be useful in solute-surface interaction studies.

Y. V. Li (✉)
Department of Design and Merchandising, Colorado State University, 326 Gifford, 1574 Campus Delivery, Fort Collins, CO 80523-1574, USA
e-mail: yan.li@colostate.edu

L. M. Cathles
Earth and Atmospheric Sciences, Cornell University, Ithaca, NY 14853, USA
e-mail: lmc19@cornell.edu

Published online: 02 March 2016

Graphical Abstract

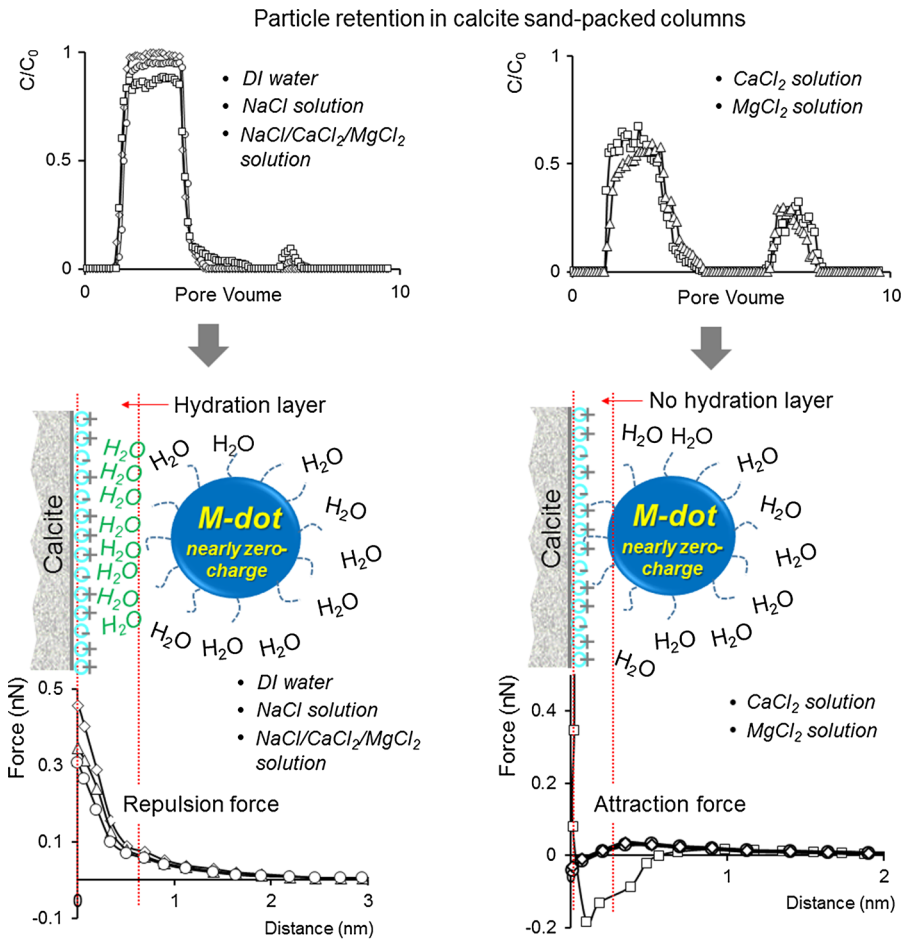

AFM force profiles between calcite probe tip and M-dot coated surface

Keywords Nanoparticle tracers · Transport · Mobility · Hydration force · Derjaguin–Landau–Verwey–Overbeek (DLVO) theory · Atomic force microscopy (AFM) · Surface science

Introduction

How fluids move in fractured aquifers, geothermal fields, and hydrocarbon reservoirs is important. Whether the fluid moves through only a few fractures or distributed through many fractures fundamentally impacts whether carbon dioxide or chemical waste can be sequestered (Pruess 2008), which strategy should be used to increase oil recovery (Fakcharoenphol et al. 2014), and how fast contaminants are transported (Essaid et al. 2015). Particle tracers have long been seen as a way to assess fracture-controlled or channelized flow because they would diffuse much less from these flow zones and comparing the arrival of particle and chemical tracers would therefore indicate the degree of channeling. The first tests of this idea were carried out in the 1970's, but the methods proved problematic (Cathles et al. 1974). Becker and Shapiro summarize the extensive theoretical and experimental work that has been done on dual chemical-particle tracer methods, showing that particles have not realized their flow characterization potential largely because they are strongly retained in laboratory

columns, rock cores, and rock and sediment formations (Becker and Shapiro 2000).

Interest in particle movement in the subsurface has been revived by the recent appreciation that contaminants may move faster through the subsurface if they attach to particles (Becker and Shapiro 2000; Rodriguez et al. 2009; Yu et al. 2010; Alaskar et al. 2011; Agenet et al. 2012; Sang et al. 2013). Our discovery of a class of carbon-cored hydrophilically decorated nanoparticles that show very little retention in porous media even when dispersed in brine with divalent cations has revived hope that dual tracer methods might yet prove effective in characterizing subsurface flow. Our previous work suggests that the inertness of these particles is mainly a consequence of their nearly neutral charge, and that the inertness is also enhanced by hydrophilic decoration and small size (Li et al. 2014).

The purpose of this paper is to investigate the interaction with calcite of one member of this class of carbon-cored hydrophilically decorated nanoparticles. The particle we use is synthesized with malic acid and ethanolamine. This carbon-cored particle (which we call M-dots) is slightly larger (11 nm) that the ~3 nm particles synthesize from citric acid and ethanolamine (C-dots) which we have found to be remarkably inert in laboratory and natural environments (Kanj 2013; Subramanian et al. 2013). Dispersed in 3.13 M mixed monovalent and divalent cation brine, 6.4 % of the M-dot particles are retained in calcite-sand-packed columns, whereas ~100 % of bare SiO_2 particles are retained (Li and Cathles 2014), and 0. % of C-dot particles are retained (Li et al. 2014). This intermediate retention of the M-dot particles provides insights that could not be obtained by studying the C-dot particles directly, and this is the reason for our choosing the M-dot particles for this study.

We use calcite as the solid media because the calcite surface, although negatively charged when in contact with DI water, develops increasingly larger areas of positive charge (associated with Ca^{2+} defects in the calcite) as the water in contact with the surface becomes more saline (Li and Cathles 2014). Electrostatic attachment of the M-dots is partially reversible. A significant portion of the retained particles are detached and flushed from the column if DI water (or water for which the particles are not retained) is passed through the column. Our hope, which was not fully realized, was that these characteristics of the particle-calcite interaction would allow better assessment of the importance of hydration forces. Differences in the hydrophilic decoration of similar nanoparticles turned out to be the best indication of the importance of hydration forces on nanoparticle retention, which hints at how useful nanoparticles could be in studying the solute-solid interface.

Below we first describe the experimental methods used, then present experimental results, and finally give our interpretation of the experimental results.

Experimental methods

Nanoparticle synthesis

The M-dots used in our experiments were synthesized by carbonization of malic acid (Sigma-Aldrich) and ethanolamine (Sigma-Aldrich) in a method similar to that described by Li et al. (2014). DI water from Milli-Q (Millipore) system was used for all reactions and solution preparations. Malic acid (268 g) was placed in a large beaker (2 L vol) containing up to 900 ml DI water. In another beaker 244 g of ethanolamine was diluted with 900 ml DI water. After complete dissolution (clear solution), the ethanolamine solution was added to the citric acid solution under constant magnetic stirring. The mixture was stirred to a homogeneous solution which is then heated to ~70 °C under constant magnetic stirring to evaporate the water. When the volume of the mixture was reduced ~500 ml, the materials were transferred to a glass bottle (1 L in volume) and further heated at ~70 °C to obtain a viscous (glue-like) material. The glue-like mixture was pyrolyzed at 200 °C in air for 8 h. The oven temperature is initially increased at a rate of 10 °C/min until 200 °C. The obtained black M-dot product was used as it was without any further purification. Figure 1 shows the M-dot synthesis reaction.

Nanoparticle characterizations

The size and morphology of M-dots were examined using a transmission electron microscopy (TEM) (FEI T12 Spirit). A droplet of 0.1 % M-dot aqueous solution was placed on a TEM grid. After the grid was dried, it was taken to TEM examinations. The images were analyzed in the image processing

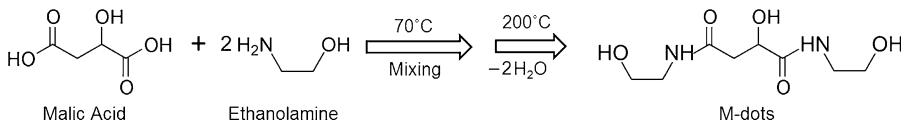

Fig. 1 Reaction scheme of malic acid and ethanolamine toward the formation of M-dots

software, ImageJ. A histogram of particle size distribution was obtained with standard deviation of particle size produced by the software.

A Zetasizer Nano system (Malvern instrument Ltd) was used to measure zeta potential of the M-dots and calcite in different electrolyte solutions. The electrolyte solutions we used in the experiments include a 2.21 M NaCl solution, a 0.74 M $CaCl_2$ solution, a 0.18 M $MgCl_2$ solution, and 3 salt mixture (2.21 M NaCl, 0.74 M $CaCl_2$, 0.18 M $MgCl_2$) that corresponds roughly to oil field production water (Li et al. 2014; Lindlof and Stoffer 1983). The zeta potential is deduced from the electrophoretic mobility of the particles measured by laser velocimetry. For measuring the zeta potential of calcite, Iceland spar (calcite from Ward's Natural Science) was ground to fine powders and then dispersed in different electrolyte solutions at a concentration of 0.005 % (by weight calcite).

The M-dot concentrations of effluent solutions were determined using a fluorescence spectrometer (SpectraMax M2^e, Molecular Devices). The peak excitation is 360 nm and the peak emission is around 460 nm. The peak emission intensity is a linear function of nanoparticle concentration below 100 ppm and the detection limit is 5 ppb. A calibration curve relating fluorescent intensity to nanoparticle concentration was established prior to each set of experiments. The injection concentration was 100 ppm in all experiments.

The pH in the M-dot electrolyte solutions was determined using an Accumet®-XL20 pH/Conductivity meter (Fisher Scientific).

Column test procedures

M-dot retention on calcite sand was measured in columns packed with 50 mesh calcite sand obtained from Specialty Mineral Inc., Lucerne Valley, CA. (see Li et al. (2014) for additional discussion of sand properties). The column consisted of a 1.8 cm of inner diameter transparent polycarbonate tube with two polycarbonate caps. The height of the sand pack in the column was ~10.1 cm, the porosity of the calcite fill was ~0.55, and the contained calcite mass was ~51 g. The pore volume (PV) of the sand pack was thus ~14.34 ml. To assure that no air was present in the water-saturated calcite sand pack, the column was first partially filled with DI water and then the sands were gradually introduced, adding DI water as needed so that the calcite was always deposited through a layer of water. The caps were attached snugly on the ends of the column with the four screws. Solutions were pumped slowly into the bottom of the column using a Masterflex® peristaltic pump (Cole Parmer) and effluent samples were collected at the top of the column using a fluid fraction collector (Frac—100, Amersham Biosciences). Prior to the injection of M-dot solutions, at least one slug of 5 PV DI water was injected to flush and fully saturate the column. Then a 2.2 PV slug of electrolyte solution containing 100 ppm M-dots was injected to the column followed by 3 PV slug of particle-free electrolyte solution, and a 5 PV DI water. Effluent was collected from the top of the column in a 2-ml plastic tube every 4 min. The flow rate through the column was 0.25 ml/min during the entire injection.

The concentration ratio (C/C_0) was plotted against the PV of injection to give breakthrough curves, where C_0 and C are the concentrations of nanoparticles in the injected nanoparticle suspension and in the effluent, respectively. Particle recovery in each column test was obtained by mass balance calculation. Each column test was repeated three times. The particle concentration in the effluent was measured to define the breakthrough curves. The three breakthrough curves were very similar and were averaged to obtain the curves shown in Figs. 3 and 4. For clarity, error bars are not displayed, as is the literature practice. However, from our data, the difference between the maximum and minimum breakthrough curves defines a spread which is typically 2 % of the average concentration. Spreads for the flat-top portions of two of the breakthrough curves are shown in Fig. 3.

AFM force measurements

Direct AFM force measurements between calcite and M-dots using a colloidal probe were made using a NTEGRA Prima, NT-MDT AFM. Because the M-dots are small ($\sim$11 nm) it is difficult to glue them on a standard AFM probe to make a colloidal M-dot probe. We therefore glued a 5-μm calcite particle to a standard AFM probe cantilever provided by Novascan Technologies. The probe had a force constant of 0.35 N/m. A silica wafer was coated with M-dot particles by immersing the wafer in a 10 wt% M-dot solution overnight, and then removing it and drying it in air. The wafer was examined under SEM and found to be covered with M-dots, with a few areas more thickly covered. Since the M-dots are 11 nm in diameter, we believe that this complete cover will assure that the AFM calcite tip will encounter an M-dot surface at a distance great enough from the silica wafer that the probe will have no force interaction with the silica surface. The AFM measured the forces between the calcite on the probe cantilever and the M-dots on the silica substrate. A liquid cell containing electrolyte solutions was used in the force measurements.

Contact angle measurements

Contact angle measurements were conducted using a Krüss DSA10 Drop Shape Analysis System Contact Angle Goniometer (CAG). The CAG measures contact angles on flat substrates using the sessile drop technique. Silica substrates (MTI Co.) were first cleaned using acetone and then immersed in an M-dot or C-dot solutions (1 % by weight) for 5 h. The treated substrates were kept under a hood and dried overnight. Contact angles were measured on a pristine silica substrate, an M-dot-coated substrate, and a C-dot-coated substrate.

DLVO theory and force fitting

The classical DLVO model we employ uses the Derjaguin approximation that improves the Van der Waals attraction (Cail and Hochella 2005). The implementation we use includes Van der Waals and electrostatic forces. The model requires specification of the diameter of the M-dots, the surface charge on the calcite and the M-dot, the dielectric constant of water, and a Hamaker constant characterizing the interaction between M-dot and calcite. The diameter of the M-dot is 11 nm (indicated by the TEM image in Fig. 2). Our zeta potential measurements show that the surface charge on the M-dot particles does not depend on the solution composition. Therefore, the surface potential of M-dot in all solutions is kept constant in the calculation. The best force fit is attained for a surface potential of – 5 mV. The surface charge on the calcite depends on the solution composition, and we treat it as a free parameter in the DLVO model. Bergström found that the pure water Hamaker constant for calcite interacting against silica is 6.9×10^{-21} N m (Bergström 1997). In this paper, we find that the Hamaker constant for the calcite AFM probe interacting against calcite that works best in interpreting our experiments is 5.0×10^{-22} N m.

The modified DLVO model includes a hydration force (Marčelja and Radić 1976). Hydration forces

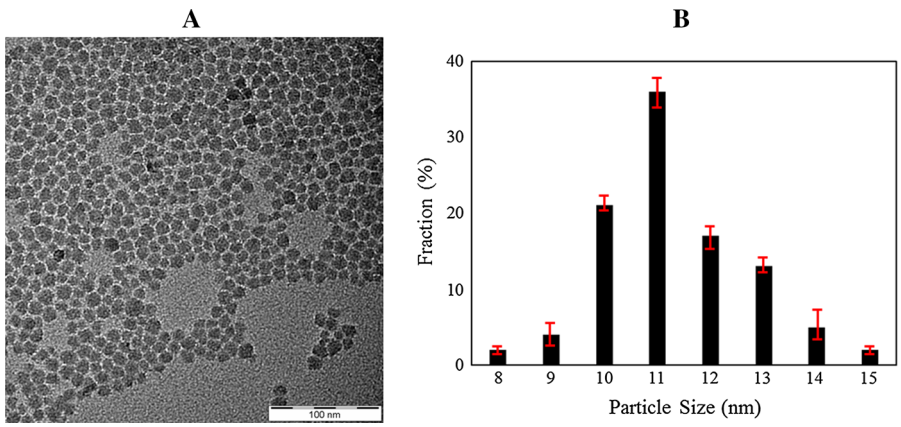

Fig. 2 A TEM image of M-dots morphology (*left*) and histogram of particle size distribution (*right*)

have been reported to play an important role in the stability of colloid and nanoparticle solutions (Marčelja and Radić 1976; Pashley and Israelachvili 1984; Ohki and Ohshima 1999; Kamiya et al. 2000; Boström et al. 2001; Raviv and Klein 2002). Marčelja and Radić (1976) developed a phenomenological model where the hydration force is described by an order parameter η (x) which depends on the distance x to the surface. This parameter is null where the system is disordered (the bulk solution) and reaches its maximum value η_0 near the surface. The hydration force, F_H, is calculated using Eq. (1),

$$F_H(x) = 2\pi R a \eta_0^2 \frac{x}{\sinh^2\left(\frac{Kx}{2}\right)} \quad (1)$$

where x is the distance from the surfaces, R is the radius of the sphere, η_0 is an order parameter which describes the order of the packed water molecules, a and K are two constants.

Results and discussion

Particle size and morphology

Figure 2 shows a TEM image of the M-dots and the corresponding particle size histogram. The TEM image shows that the M-dots average 11 nm in diameter, are nearly spherical, and are well dispersed in water. The particle size is similar to carbon nanoparticles synthesized by other routes whose average diameters range from 4 to 10 nm (Cao et al. 2007; Bourlinos et al. 2008; Ray et al. 2009; Pan et al. 2010). For example, Krysmann et al. (2012) heated and prolysized the mixture of ethanolamine and citric acid at 300 °C and obtained carbon nanoparticles that had an average particle diameter of 8 nm. Our standard C-dot nanoparticles have a mean diameter of ~3 nm (Subramanian et al. 2013).

Particle fluorescence properties

The M-dots have a peak excitation at 360 nm and a peak emission peak at ~460 nm. Carbon nanoparticles synthesized from ethanolamine and citric acid (C-dots) have a peak excitation of 375 nm and a peak emission of 455 nm. The C-dot particles are 37 % more fluorescent than the M-dots at 100 ppm concentration when both were measured just after synthesis.

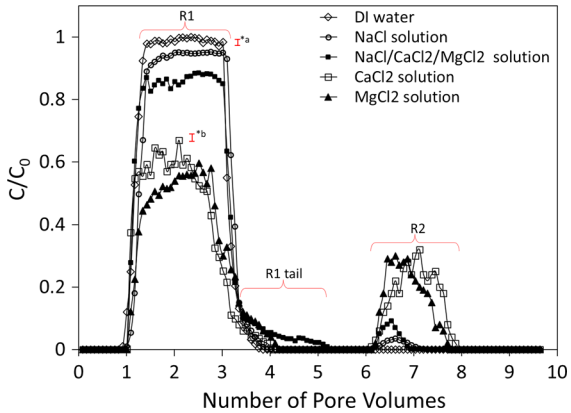

Fig. 3 M-dot concentration in the column effluent normalized by the injected concentration in water and salt solutions is plotted as a function of the number of pore volumes injected. In all cases, a slug of 2.2 PV of M-dot solution is followed by 3 PV of particle-free solution and then 5 PV of DI water. In cases where the M-dots are retained, the DI water flushes out the retained M-dots, producing a secondary arrival pulse

Retention of M-dots in calcite sand-packed column

Figure 3 shows the ratio of collected to injected M-dot concentration (C/C_0) as a function of the number of PV of solution passed through the calcite wet sand-packed column. For all solution compositions, the M-dots were first detected at ~0.9 PV and the M-dot effluent concentration increased sharply at ~1 PV injection. Table 2 lists the percentages of injected particles retained and releases in various portions of these curves. When dispersed in DI water, the M-dot effluent concentration curve is a box-like pulse across which 99.6 % of the injected particles are recovered. When dispersed in either the 2.21 M NaCl solution or the mixed salt solution (2.21 M NaCl, 0.74 M $CaCl_2$, and 0.18 M $MgCl_2$), the effluent concentration curve remains box-like but the maximum concentration is depressed, and 4.5 and 7.6 % of the particles are retained in the column, respectively. Most of these retained M-dots are recovered when the column is flushed with DI water, but about 2.3 % of the particles are not recovered. When the particles are dispersed in divalent salt solutions (0.74 M $CaCl_2$ or 0.18 M $MgCl_2$), almost 50 % of the particles are initially retained, but later recovered by the DI flush. The M-dot concentration begins to drop before the end of the injection pulse and there is a significant concentration tail. For the $MgCl_2$ solution, the initial arrival pulse is not flat-topped. When the M-dots are

dispersed in the mixed brine containing NaCl as well as the same concentrations of $CaCl_2$ and $MgCl_2$ as in the experiments with these individual salts, the curve is again box-shaped but there is a more extensive tail than the other experiments. Including the tail about 7.6 % of the particles are retained, 67 % of which are recovered in the DI flush.

Figure 4 shows that C-dots are much less retained than the M-dots in the calcite sand-packed column when dispersed in the same mixed brine. The column design and the experimental procedures of the two column tests are the same. Bare silica nanoparticles dispersed in the brine (curve not shown) are entirely retained in the column under these same conditions (Kanj 2013). The C-dots were synthesized from citric acid and ethanolamine rather than malic acid and ethanolamine. The C-dots and M-dots are chemically similar and both have the same zeta potential within measurement error. However, the C-dots (3 nm) are smaller in diameter than the M-dots (11 nm).

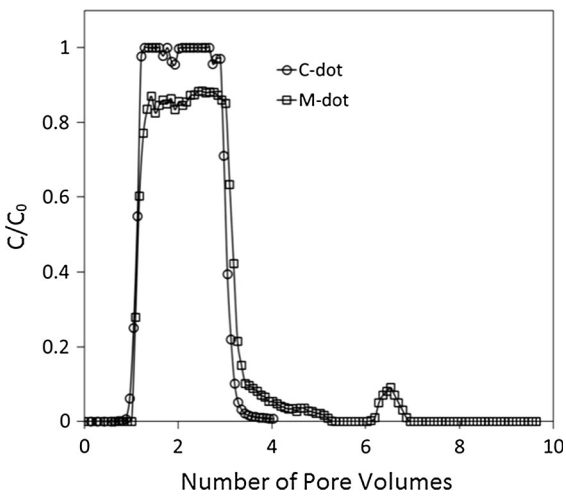

Fig. 4 Comparison of the M-dot and C-dot effluent arrival curves when both particles are dispersed in an identical NaCl/$CaCl_2$/$MgCl_2$ brine (see Table 1). The M-dot curve is from Fig. 3; the C-dot curve is from Li et al. (2014). The M-dot particles show retention whereas the C-dot particles do not. The injection protocol is described in the caption of Fig. 3

Zeta potentials

The zeta potentials of the M-dots dispersed in the different solutions are shown in Table 1. The zeta potentials of the M-dots are slightly negative and independent of the solution water chemistry. This is in agreement with carbon nanoparticles prepared in various methods (Wang et al. 2011; Qin et al. 2013). The calcite surface is negatively charged in DI water (-14.5 ± 0.8 mV, less negatively charged in NaCl solution (-8.5 ± 0.9 mV), and slightly negatively charged in the mixed brine. The calcite has a strongly positive zeta potential when immersed in the $CaCl_2$ and $MgCl_2$ solutions. The C-dots have a smaller zeta potential in the mixed brine and DI water than the M-dots, but the error bar on the measurements is large.

AFM force profiles

The interfacial forces between M-dots and calcite sand measured using AFM are shown in Fig. 5. When the calcite colloidal probe approaches the bare silica substrate immersed in water, after a slight repulsion force (0.02 nN) a strong attraction (0.2 nN) is measured beginning at about 0.6 nm. When the calcite probe approaches an M-dot coated substrate immersed in water, however, there is no attraction, only strong repulsion. This is also true for the NaCl and mixed brine solutions. For the $CaCl_2$ and $MgCl_2$ solutions, there is a weak initial repulsion followed by a small attraction starting at $\sim$0.01 nN.

Table 1 Zeta potentials (mV) of M-dots, C-dots (Li et al. 2014) and calcite in aqueous solutions

Solution	M-dots		C-dots		Calcite	
	Zeta potentials	pH	Zeta potentials	pH	Zeta potentials	pH
DI water	-2.8 ± 0.9	7.52	-1.5 ± 2.0	7.35	-14.5 ± 0.8	8.29
NaCl solution (2.21 M)	-2.1 ± 1.1	6.75	–	–	-8.5 ± 0.9	7.53
$CaCl_2$ solution (0.74 M)	-2.5 ± 1.2	6.62	–	–	7.1 ± 1.5	6.89
$MgCl_2$ solution (0.18 M)	-2.4 ± 1.5	6.77	–	–	9.8 ± 1.1	8.81
Mixture solution (2.21 M NaCl, 0.74 M $CaCl_2$, 0.18 M $MgCl_2$)	-2.3 ± 1.0	6.85	-0.88 ± 3.4	6.34	-0.5 ± 1.6	6.14

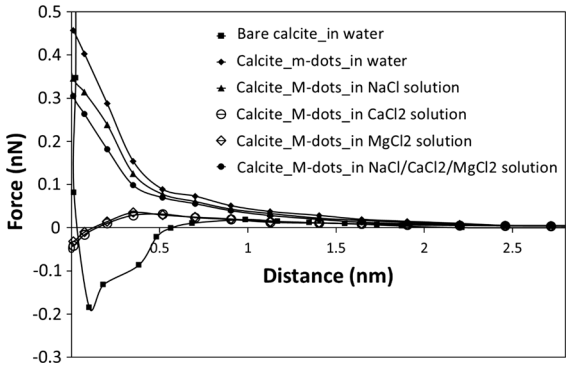

Fig. 5 AFM force measurements of a calcium carbonate colloidal AFM probe approaching a bare silica substrate and a silica substrate coated with M-dots when submerged in water, and NaCl, $CaCl_2$, $MgCl_2$, and mixed $NaCl/CaCl_2/MgCl_2$ salt solutions with concentrations given in Table 1. The uncertainties in the force curve measurements are small compared to the differences between the curves. The close overlap of the M-dot curves for the $CaCl_2$ and $MgCl_2$ provides an indication of the force uncertainty

Contact angle measurements

The hydrophilicity of M-dots and C-dots was evaluated by the contact angle measurements as shown in Fig. 6. The C-dot surface has a highly hydrophilic contact angle of 32° ± 1.2° while the M-dot surface has a much less hydrophilic contact angle of 54° ± 0.8°, and the bare silica surface an only slightly hydrophilic contact angle of 88° ± 0.5°. Both M-dot and C-dot increase the hydrophilicity of the substrate, but the C-dot surface is the most hydrophilic.

DLVO analysis of the AFM force curves

Table 2 shows that the DLVO model that is modified to include hydration forces successfully predicts the force between the AFM calcite tip and the M-dot surface at a distance of 0.1 nm when the surface and probe are submerged in DI water, NaCl, or the mixed solutions. The table shows, however, that the classical DLVO model predicts the force of interaction for the $CaCl_2$ and $MgCl_2$ solutions. Figure 7 shows the quality of the modified DLVO model fit to the force curve for DI water, and also shows the stark difference in the predictions of the classical and modified DLVO models. The Hamaker constant for the calcite probe that works best in interpreting the force profiles for both the classical and modified DLVO models is 5.0×10^{-22} N m. The hydration parameters which provide the best fit are $a\eta_0^2 = 8.2 \times 10^5$ N/m^2 and $K = 2.5$ nm^{-1}.

Our best hydration force fitting parameters are similar to those reported by Valle-Degado et al. (2005) found best for fitting force curves between silica surfaces in 1 M NaCl solution ($a\eta_0^2 = 6.8 \times 10^5$ N/m^2, $K = 2.5$ nm^{-1}). Our larger value suggests that our

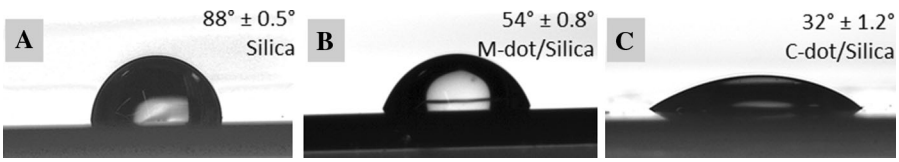

Fig. 6 Shows the shape of a DI water droplet on **a** a silica surface, **b** a silica surface coated with M-dots, and **c** a silica surface coated with C-dots

Table 2 Particle recovery (R1, R1 tail, and R2, %, see Fig. 3), permanent particle retention R^* (%), and interfacial forces (nN) measured by AFM (F1) and predicted by DLVO models (F2 from classical DLVO, and F3 from modified DLVO) at distance = 0.05 nm in the solutions

Solution	$R1$ (%)	$R1$ tail (%)	$R2$ (%)	R^* (%)	$F1$	$F2$	$F3$
DI water	98.3 ± 0.2	1.7 ± 0.1	0.15 ± 0.15	0	0.41	−0.25	0.42
NaCl	92.4 ± 0.5	2.1 ± 0.3	1.9 ± 0.3	3.6 ± 1.1	0.27	−0.42	0.29
$NaCl/CaCl_2/MgCl_2$	86.9 ± 0.6	5.8 ± 0.3	0.9 ± 0.2	6.4 ± 1.1	0.32	−0.45	0.33
$CaCl_2$	54.0 ± 1.5	2.0 ± 0.9	15.0 ± 1.1	30.0 ± 4.5	−0.031	−0.032	0.75
$MgCl_2$	52.0 ± 0.7	2.1 ± 0.2	13.8 ± 0.6	32.1 ± 1.5	−0.029	−0.035	0.76

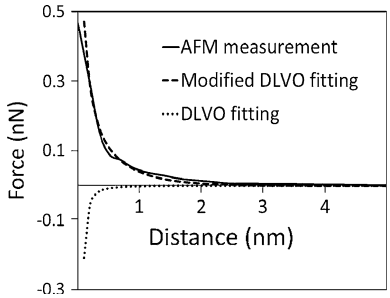

Fig. 7 The AFM force profile measured as the calcite tip of an AFM probe approaches an M-dot-coated silica surface immersed in DI water (*solid line*) is compared to the force profile predicted by a DLVO model that is modified to take hydration forces into account (*thick dash line*) and the force profile predicted by the classical DLVO model (*thin dashed lines*) that does not include hydration forces. The modified DLVO model matches the measurements very well whereas the unmodified classical DLVO model fails completely

water thin film may be slightly more densely packed and ordered near the M-dot coated surface than Valle-Degado et al.'s film was near their silica surface. Our DLVO Hamaker constant of 5.0×10^{-22} N m is below the lower end of the typical range of 10^{-21} to 10^{-19} N m for this parameter [Israelachvili 1985]. We have previously found Hamaker constants for calcite interacting with silica in NaCl and Na_2SO_4 solution (1.74×10^{-21} and 1.50×10^{-21} N m for the NaCl and Na_2SO_4 solutions, respectively) (Li and Cathles 2014). The low Hamaker constant suggests the Van der Waals interaction between M-dot and calcite is smaller than between silica and calcite. Table 2 indicates that the total interfacial force in NaCl solution predicted by our modified DLVO modeling is 0.33 nN. This is larger than the force between a silica particle and a silica surface of 0.12 nN determined by Fielden et al. (2000), which suggests that the M-dot hydration may be particularly strong.

For the interactions when the surfaces are submerged in $CaCl_2$ and $MgCl_2$ solutions (not shown) the opposite is the case—the classical model fits the observations well and the modified DLVO model fails.

Particle retention and surface interactions

The zeta potential of calcite is the primary factor controlling M-dot retention in the calcite sand-packed column. The zeta potential of the M-dots is similar in all the solutions (about −2.5 mV), but, as shown in Table 1, the zeta potential of the calcite changes as a function of solution composition from strongly negative to positive, and the retention in the column experiments tracks this change. In all cases, the retention is significantly reversible. No M-dots are retained when dispersed in DI water, and flooding with DI water recovers a significant proportion of the M-dots that are retained in the column when they are dispersed in the other solutions. This indicates that an important part of the particle retention is due to electrostatic attraction. Our interpretation is that the M-dot particle with small negative charge is retained on the positively charged portions of the calcite surface that develop and increase in area when the calcite is in contact with progressively more saline solutions (Li and Cathles 2014). These retained particles are released when DI water replaces these solutions and the areas of positive charge on the calcite surface disappear. The attachment mechanism for the permanently retained particles is not clear.

The tail on the particle injection pulse is more substantial for the M-dots dispersed in the mixed brine. The retention during the pulse is 13.1 % of the injected particles, but almost half of these are flushed out in the tail, and a bit more when the column is flushed with DI water; 6.4 % of the injected particles are "permanently" retained (Fig. 3; Table 2). The recovery tail for the mixed brine experiment contains more than twice the percentage of injected particles than any of the other experiments, all of which are similar (Table 2). The electrostatic retention seems to be weaker for the mixed brine.

Hydration forces are the probably explanation for the greater tail recovery in the mixed brine, but the story is complicated and highlights the special role of the Na^+ ion, and requires extended discussion. The story is complicated primarily because both the hydrophilic particle decoration and the hydration introduced by ions in the double layer adjacent to the calcite surface are important to the hydration repulsion of the particles. The dense, ordered water produced by the ethanolamine decoration on the M-dots produces a strong hydration force when the M-dots approach the calcite surface and encounter the hydration spheres of ions in the bound water layer near the surface. This keeps the M-dots away from the Van der Wall attraction well and reduces electrostatic adhesion.

Hydration forces are probed most directly by the AFM measurements (Table 2) and the associated DLVO modeling of the AFM force profiles. The force profiles measured when the M-dot-coated calcite surface is submerged in DI water, or in any of the solutions that contain Na^+ ions, indicate that a strong repulsive hydration force is present close to the calcite surface. Figure 8 (left) illustrates the proposed hydration layer structure between an M-dot and calcite surface. A DLVO model that is modified to account for these forces is required to interpret the force profiles (Table 2), and the hydration parameters for all these best-fitting interpretive models are the same. On the other hand, the divalent cation (Ca^{2+} or Mg^{2+}) solutions that contain no Na^+ ions show no hydration repulsion of the calcite probe, as illustrated in Fig. 8 (right). The force curves for the $CaCl_2$ and $MgCl_2$ solutions are fit by the classical DLVO theory that does not contain hydration forces, and the force curves cannot be fit when hydration forces are included in the DLVO model. A surprising observation is that when the M-dot coated surface is submerged in a salt solution consisting of $MgCl_2$, $CaCl_2$, and NaCl, the hydration forces return. The presence of NaCl in a mixture of brines which individually show no hydration repulsion turns the hydration repulsion back on.

Some of these relations are expected from previous studies of silica and clay surface interactions. Sodium ions are strongly hydrated in NaCl solution (Fielden et al. 2000). Calcium and magnesium ions are even more strongly hydrated. When any of these cations are present in the water layer adjacent to a surface they contribute their hydration forces there (Pashley 1981; Horn et al. 1989; Ducker et al. 1991; Saraji et al. 2013). This near-surface hydration is "switched off," however, when the concentration of Ca^{2+} or Mg^{2+} or the pH increase above some threshold. Meagher (1992) showed the hydration force is switched off for silica surfaces when the $CaCl_2$ concentration is greater than 1 M at a pH of 5.3, but did not constrain a lower bounds of concentration or pH for the switch off. Our results indicate the hydration force adjacent to a calcite surface is removed when the $CaCl_2$ concentration is greater than 0.74 M at a pH of 6.89. We also do not determine the lower bounds of the switch off, but our results are clearly very similar to Meaghan's. It has been suggested that the hydration force is turned off by the increased columbic attraction induced of the bivalency of the salt cations (Hunter 1986; Fielden et al. 2000). Bivalent bridging between surfaces (Ralston et al. 1981) or ion-correlations (Kjellander and Marčelja 1984; Attard et al. 1988) seem to be involved because the pull-off force of an AFM probe is greater than that expected from the Van der Waals force alone, and additional attractive forces are therefore required (Valle-Delgado et al. 2005). For Na^+ ions, the hydration forces are never switched off and it is impossible to bind silica or mica surfaces if they are pressed together submerged in ~0.01 M or greater NaCl solutions (Pashley 1981; Horn et al. 1989; Ducker et al. 1991; Saraji et al. 2013).

The AFM measurements summarized in Table 2 are thus compatible with previous studies on clays and silica. That the hydration force switch off occurs at such similar $CaCl_2$ concentrations for silica and calcite surfaces suggests that the switch off is controlled by the solution chemistry near the solid surface alone and is not dependent on the nature of the solid surface. What is surprising in our results, and so far as we know is a new observation, is that the hydration force is preserved by the addition NaCl to a mixed salt solution whose $MgCl_2$ and $CaCl_2$ concentrations are each individually sufficient to switch it off. Evidently Na^+ is able to suppress the impact of the divalent cations in the salt mixture and preserve the surface hydration. Discussion of the suppression mechanism is beyond the scope of this paper, but it seems to be quite complete. The AFM force measurements for the 2.1 M NaCl solution and the mixed salt solution are very

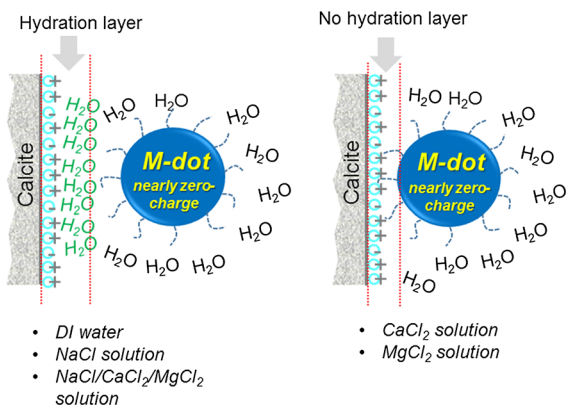

Fig. 8 A scheme of hydration layer and force between an M-dot and calcite when dispersed in DI water, NaCl solution, or $NaCl/CaCl_2/MgCl_2$ mixture solution (*Left*). No hydration layer is constructed when the M-dot and calcite are immersed in a $CaCl_2$ or $MgCl_2$ solution (*Right*)

similar (Table 1), which indicates that the presence of Ca^{+2} and Mg^{+2} ions has remarkably little impact on the Na^{+}-associated hydration. Their only impact seems to be the larger permanent particle retention (6.4 % for the mixed compared to 3.6 % for the NaCl brine) and the larger recovery tail for the mixed brine. The interaction of the M-dots with the calcite surface seems to be more complex in the mixed brine case, allowing the weak temporary attachment that is responsible for the larger recovery tail.

The importance the hydration forces is suggested by the fact that the small retentions of M-dots in the NaCl and mixed brine solutions are similar despite the very much more negative zeta potential of the calcite submerged in NaCl compared to calcite submerged in the mixed brine (Table 1). All else being equal, the more negative zeta potential of the calcite should mean more M-dots are electrostatically retained when dispersed in the NaCl brine, but they are not. The AFM measurements show that the hydration-dominated force profiles are similar for NaCl and mixed brine solutions supporting the conclusion that hydration forces are the cause of low particle retention in both cases.

Other evidence supports the importance of hydration forces. C-dot particles synthesized from citric acid and decorated with ethanolamine are not retained at all in the mixed brine (Fig. 4), whereas 13.1 % of the M-dot particles are temporarily and 6.4 % are permanently retained (Fig. 3; Table 2). The contact angle measurements shown in Fig. 6 show that the C-dots are dramatically more hydrophilic than the M-dots. Thus, hydration increases the inert character of the C-dot compared to the M-dot nanoparticles. Previous experiments reinforce this conclusion. For example, carbon-cored particles synthesized from citric acid but decorated with slightly less hydrophilic jeffamine are retained more than similar size particles decorated with ethanolamine (Li et al. 2014). Although the error bars are large, the zeta potential of the C-dots in DI water and in the mixed brine seems to be less than the M-dots (Table 1). Our interpretation is that the more complete hydrophilic decoration of the C-dot particles results in the lower zeta potential and therefore we attribute the more inert character of the C-dots to superior hydrophilic decoration. The possibility that the changes in decoration changed the charge of particles and that a more neutral charge on the C-dots is responsible for their greater inertness should be kept in mind, however.

The greater hydrophilicity of the C-dot particles is expected. The amine groups on the ethanolamine are the source of the particle hydrophilicity (Yan et al. 2006; Gu et al. 2011; Krysmann et al. 2012). The amine groups attract water molecules and promote the formation of a structured water film where water molecules are densely packed (Argyris et al. 2008; Barnette et al. 2008). The only difference in the synthesis of the C-dot and M-dot particles is the use of malic acid in the synthesis of the M-dots instead of citric acid in the synthesis of the C-dots (Krysmann et al. 2012; Li et al. 2014). Malic acid has two carboxyl (−COOH) groups and citric acid has three. Ethanolamine attaches to the carboxyl groups. If complete, the ethanolamine decoration is thus 50 % greater for the C-dot particles compared to the M-dot particles, and the C-dots should be more hydrophilic than the M-dot particles as indicated by the contact angle measurements. Since the ethanolamine decoration is the main source of fluorescence (Li et al. 2014) [although there could be some contribution from the carbon core itself (Krysmann et al. 2012)], the C-dot particles should also be more fluorescent than the M-dot particles. The greater ethanolamine decoration could more than account for the observed 37 % greater fluorescence of the C-dot compared to M-dot nanoparticles.

We expect that nanoparticles at the 100 ppm concentrations used in our experiments have very little impact on the solution chemistry. Changing particles should therefore not change the zeta potential of calcite or the ion concentrations or their hydration near the calcite surface. Changing the particles should only change the hydration forces surrounding the particles. Thus, comparing the retention of similar particles with different hydrophilic decorations is a way to assess the importance of hydration forces near a surface isolated from other factors. Changing solution composition changes both the zeta potential of the calcite and the hydration near the solid surface, but changing the decoration on the nanoparticles changes only the hydration interaction with the solid surface.

Conclusion

The retention of carbon-cored hydrophilically decorated nanoparticles synthesized from malic acid and ethanolamine in calcite sand-packed laboratory columns depends

on the chemistry of the water in which the particles are dispersed when they are passed through the column. There is no retention when the particles are dispersed in DI water, but there is significant retention when the particles are dispersed in 2.1 M NaCl or a mixed brine of 2.1 M NaCl + 0.74 $CaCl_2$ + 0.18 M $MgCl_2$, and more than half of the nanoparticles are retained when dispersed in 0.74 M $CaCl_2$ or 0.18 M $MgCl_2$ salt solutions. About 35 % of the particles retained from the NaCl brine and 25 % of the particles retained from the $CaCl_2$ and $MgCl_2$ brines are released when the column is flushed with DI water. The tail following the termination of particle injection is twice as big for the mixed brine as in the other cases, suggesting a weaker electrostatic retention which is consistent with the negative zeta potential being much smaller in magnitude in the mixed brine. The AFM force profiles between a calcite probe and an M-dot coated surface indicate nearly identical hydration repulsion for the NaCl and mixed brine solutions. Since the much more negative zeta potential of calcite contacting the NaCl solution should produce greater retention, hydration forces seem to be the dominant cause of particle inertness in these solutions.

The AFM force profiles between a calcite-tipped probe and an M-dot coated surface indicate that there are strong hydration forces repelling the calcite tip in the DI water, NaCl, and mixed brine cases, but there are no repulsive hydration forces in the $CaCl_2$ and $MgCl_2$ solutions. The zeta potential of calcite in the $CaCl_2$ and $MgCl_2$ solutions is strongly positive, so the greater retention of the weakly negatively charged M-dots is the consequence of some combination of the positive surface charge of the calcite of the absence of repulsive hydration forces in these solutions. The changes in solution chemistry affect both the calcite zeta potential and the hydration near the calcite surface, so the effects cannot be separated.

The hydration near the nanoparticles can be modified by changing the density of their hydrophilic decoration. C-dot nanoparticles synthesized with citric acid have 50 % more carboxyl sites where the hydrophilic and fluorescent ethanolamine can attach. The contact angle of DI water on a C-dot-coated surface is 32° ± 1.2° and on an M-dot-coated surface 54° ± 0.8°. The C-dots are thus much more hydrophilic than the M-dots, and they are also 37 % more fluorescent. The complete lack of retention of the C-dot particles in calcite sand-packed column when dispersed in the mixed brine compared to the over 6.4 % retention of the M-dots under the same conditions indicates the importance of hydration forces in reducing particle retention.

The experiments reported here indicate that the reason for the surprisingly low retention of carbon-cored hydrophilically decorated nanoparticles is their near zero zeta potential and highly hydrophilic decoration. The experiments also indicate the potential utility of highly engineerable nanoparticles in studies of the solute-solid interface. The properties of this interface are complicated because solution chemistry affects both the surface charge and its hydration. The surprising ability of Na^+ to preserve calcite hydration in divalent cation solutions in our experiments is an example of the questions that remain. The ability to change the hydrophilicity of nanoparticles without significantly impacting the solution chemistry allows hydration interactions to be interrogated independently. Although our understanding of carbon-cored nanoparticle inertness is substantially advanced by the work we report here, important questions remain for future investigation, most importantly perhaps the origin of charge in the carbon-cored particles and whether hydrophilic decoration in changing this charge or simply shielding it more effectively.

Acknowledgments This publication is based on work supported by Award No. KUS-C1-018-02 from the King Abdullah University of Science and Technology and by ARI project from Department of Energy. Support was also provided by a general fund contribution to L. Cathles from The International Research Institute of Stavanger.

References

Agenet N, Perriat, P, Brichart T, Crowther N, Martini M, Tillement O (2012) Fluorescent nanobeads: a first step toward intelligent water Tracers. In: SPE international oilfield nanotechnology conference and exhibition. doi:10.2118/157019-MS

Alaskar M, Ames M, Connor S, Liu C, Cui Y, Li K, Roland H (2011) Nanoparticle and microparticle flow in porous and fractured media: an experimental study. In: SPE annual technical conference and exhibition. doi:10.2118/146752-PA

Argyris D, Tummala NR, Striolo A, Cole DR (2008) Molecular structure and dynamics in thin water films at the silica and graphite surfaces. J Phys Chem C 112(35):13587–13599

Attard P, Mitchell DJ, Ninham BW (1988) Beyond Poisson–Boltzmann: images and correlations in the electric double layer. I. Counterions only. J Chem Phys 88(8):4987–4996

Barnette AL, Asay DB, Kim SH (2008) Average molecular orientations in the adsorbed water layers on silicon oxide in ambient conditions. Phys Chem Chem Phys 10(32):4981–4986

Becker MW, Shapiro AM (2000) Tracer transport in fractured crystalline rock: evidence of nondiffusive breakthrough tailing. Water Resour Res 36(7):1677–1686

Bergström L (1997) Hamaker constants of inorganic materials. Adv Colloid Interface Sci 70:125–169

Boström M, Williams DRM, Ninham BW (2001) Specific ion effects: Why DLVO theory fails for biology and colloid systems. Phys Rev Lett 87(16):168103

Bourlinos AB, Stassinopoulos A, Anglos D, Zboril R, Georgakilas V, Giannelis EP (2008) Photoluminescent carbogenic dots. Chem Mater 20(14):4539–4541

Cail TL, Hochella MF (2005) Experimentally derived sticking efficiencies of microparticles using atomic force microscopy. Environ Sci Technol 39(4):1011–1017

Cao L et al (2007) Carbon dots for multiphoton bioimaging. J Am Chem Soc 129(37):11318–11319

Cathles LM, Spedden HR, Malouf EE (1974) A tracer technique to measure the diffusional accesability of matrix block mineralization. In: 103rd AIME annual meeting, The American Institute of Mining, Metallurgical, & Petroluem Engineers, Inc., Dallas, Texas, pp. 73–94005

Ducker WA, Senden TJ, Pashley RM (1991) Direct measurement of colloidal forces using an atomic force microscope. Nature 353(6341):239–241

Essaid HI, Bekins BA, Cozzarelli IM (2015) Organic contaminant transport and fate in the subsurface: Evolution of knowledge and understanding. Water Resour Res 51:4861–4902

Fakcharoenphol P, Kurtoglu B, Kazemi H, Charoenwongsa S, Wu Y.-S (2014) The effect of osmotic pressure on improve oil recovery from fractured shale formations. In: SPE unconventional resources conference, doi:10.2118/168998-MS

Fielden ML, Hayes RA, Ralston J (2000) Oscillatory and ion-correlation forces observed in direct force measurements between silica surfaces in concentrated $CaCl_2$ solutions. Phys Chem Chem Phys 2(11):2623–2628

Gu J, Su S, Li Y, He Q, Shi J (2011) Hydrophilic mesoporous carbon nanoparticles as carriers for sustained release of hydrophobic anti-cancer drugs. Chem Commun 47(7):2101–2103

Horn RG, Smith DT, Haller W (1989) Surface forces and viscosity of water measured between silica sheets. Chem Phys Lett 162(4–5):404–408

Hunter RJ (1986) Foundations of colloid science. Oxford University Press, Oxford

Israelachvili J (1985) Intermolecular and surface forces. Academic Press Inc, Cambridge

Kamiya H, Mitsui M, Takano H, Miyazawa S (2000) Influence of particle diameter on surface silanol structure, hydration forces, and aggregation behavior of alkoxide-derived silica particles. J Am Ceram Soc 83(2):287–293

Kanj M (2013) Reservoir nanoagents for in-situ sensing and intervention. In: Mavroidis C, Ferreira A (eds) Nanorobotics. Springer, New York, pp 51–67

Kjellander R, Marcělja S (1984) Correlation and image charge effects in electric double layers. Chem Phys Lett 112(1):49–53

Krysmann MJ, Kelarakis A, Dallas P, Giannelis EP (2012) Formation mechanism of carbogenic nanoparticles with dual photoluminescence emission. J Am Chem Soc 134(2):747–751

Li YV, Cathles LM (2014) Retention of silica nanoparticles on calcium carbonate sands immersed in electrolyte solutions. J Colloid Interface Sci 436:1–8

Li YV, Cathles LM, Archer L (2014) Nanoparticle tracers in calcium carbonate porous media. J Nanopart Res 16(8):1–14

Lindlof JC, Stoffer KG (1983) A case study of seawater injection incompatibility. J Pet Technol 35(7):1256–1263

Marčelja S, Radić N (1976) Repulsion of interfaces due to boundary water. Chem Phys Lett 42(1):129–130

Meagher L (1992) Direct measurement of forces between silica surfaces in aqueous $CaCl_2$ solutions using an atomic force microscope. J Colloid Interface Sci 152(1):293–295

Ohki S, Ohshima H (1999) Interaction and aggregation of lipid vesicles (DLVO theory versus modified DLVO theory). Colloids Surf B 14(1–4):27–45

Pan D, Zhang J, Li Z, Wu C, Yan X, Wu M (2010) Observation of pH-, solvent-, spin-, and excitation-dependent blue photoluminescence from carbon nanoparticles. Chem Commun 46(21):3681–3683

Pashley RM (1981) DLVO and hydration forces between mica surfaces in Li^+, Na^+, K^+, and Cs^+ electrolyte solutions: a correlation of double-layer and hydration forces with surface cation exchange properties. J Colloid Interface Sci 83(2):531–546

Pashley RM, Israelachvili JN (1984) DlVO and hydration forces between mica surfaces in Mg^{2+}, Ca^{2+}, Sr^{2+}, and Ba^{2+} chloride solutions. J Colloid Interface Sci 97(2):446–455

Pruess K (2008) On CO_2 fluid flow and heat transfer behavior in the subsurface, following leakage from a geologic storage reservoir. Environ Geol 54(8):1677–1686

Qin X, Lu W, Asiri AM, Al-Youbi AO, Sun X (2013) Microwave-assisted rapid green synthesis of photoluminescent carbon nanodots from flour and their applications for sensitive and selective detection of mercury(II) ions. Sens Actuators B 184:156–162

Ralston J, Van Vliet T, Lyklema J (1981) Inference on ion binding to polyelectrolytes from emulsion rheology. J Colloid Interface Sci 82(1):53–61

Raviv U, Klein J (2002) Fluidity of bound hydration layers. Science 297(5586):1540–1543

Ray SC, Saha A, Jana NR, Sarkar R (2009) Fluorescent carbon nanoparticles: synthesis, characterization, and bioimaging application. J Phys Chem C 113(43):18546–18551

Rodriguez, E., M. R. Roberts, H. Yu, C. Huh, S. L., and S. Bryant (2009), Enhanced Migration of Surface-Treated Nanoparticles in Sedimentary Rocks. In: SPE annual technical conference and exhibition, Society of Petroleum Engineers. doi: 10.2118/124418-MS

Sang W, Morales VL, Zhang W, Stoof CR, Gao B, Schatz AL, Zhang Y, Steenhuis TS (2013) Quantification of colloid retention and release by straining and energy minima in variably saturated porous media. Environ Sci Technol 47(15):8256–8264

Saraji S, Goual L, Piri M (2013) Dynamic adsorption of asphaltenes on quartz and calcite packs in the presence of brine films. Colloids Surf A 434:260–267

Subramanian SK, Li Y, Cathles LM (2013) Assessing preferential flow by simultaneously injecting nanoparticle and chemical tracers. Water Resour Res 49(1):29–42

Valle-Delgado JJ, Molina-Bolivar JA, Galisteo-Gonzalez F, Galvez-Ruiz MJ, Feiler A, Rutland MW (2005) Hydration forces between silica surfaces: experimental data and predictions from different theories. J Chem Phys 123(3): 034708

Wang X, Qu K, Xu B, Ren J, Qu X (2011) Microwave assisted one-step green synthesis of cell-permeable multicolor photoluminescent carbon dots without surface passivation reagents. J Mater Chem 21(8):2445–2450

Yan A, Lau BW, Weissman BS, Külaots I, Yang NYC, Kane AB, Hurt RH (2006) Biocompatible, hydrophilic, supramolecular carbon nanoparticles for cell delivery. Adv Mater 18(18):2373–2378

Yu H, Kotsmar C, Yoon KY, Ingram DR, Johnston KP, Bryant SL, Huh C (2010) Transport and retention of aqueous dispersions of paramagnetic nanoparticles in reservoir rocks. In: SPE improved oil recovery symposium, society of petroleum engineers. doi: 10.2118/129887-MS